RSC Advances

ROYAL SOCIETY OF CHEMISTRY

www.rsc.org/advances

RSC Advances

ARTICLE

High photocatalytic activity of carbon doped TiO_2 prepared by fast combustion of organic capping ligands

Received 00th January 20xx,
Accepted 00th January 20xx

DOI: 10.1039/x0xx00000x

www.rsc.org/

Yijun Yang,[a] Dawei Ni,[b] Ye Yao,[b] Yeteng Zhong,[a] Ying Ma,*[b] and Jiannian Yao*[a]

Carbon doping has been widely applied to modify TiO_2 to improve photocatalytic activity and initiate visible light activity. Using oleylamine wrapped TiO_2 nanomaterials as precursor, carbon doped TiO_2 photocatalysts have been synthesized by control of heating ramp rates and temperatures in air. Optical absorption of all these photocatalysts are extended to visible light, and photogenerated electron-hole separation is enhanced by carbon doping. Especially, those prepared by fast combustion of oleylamine ligands exhibit excellent photocatalytic activity and visible light activity for hydrogen production. EPR analysis demonstrates that more oxygen vacancies present in carbon doped TiO_2 with high activity. This indicates that oxygen vacancies may play key roles in photocatalytic water splitting. Fast heating process may have offered an oxygen-poor atmosphere in which oxygen vacancies are favoured.

Introduction

As a semiconductor photocatalyst, TiO_2 has been extensively investigated for decades because of its outstanding stability, environmental friendliness and low cost.[1-3] Many efforts have been made to improve its photocatalytic efficiency by extending its absorption to visible light or promoting photogenerated electron-hole separation on its surface.[4-6] Especially, improving absorption in visible range is very important for application considering that only about 4% solar light can be used to excite TiO_2.[7] Since Asahi et al. demonstrated band-gap narrowing and high photocatalytic activity under visible light of nitrogen doped TiO_2,[8] non-metal doping has been widely applied to modify band-gap structure of TiO_2 to initiate visible light activity.[9]

In addition to nitrogen[10, 11], carbon has also been well accepted as an efficient doping element to make TiO_2 sensitive to visible light. Khan[12] et al. firstly reported that $TiO_{2-x}C_x$ (x ~ 0.15) absorbed light at wavelengths below 535 nm and performed water splitting at an applied potential of 0.3 V. Sakthivel and Kisch found good photocatalytic property of carbon doped TiO_2 in degradation of 4-chlorophenol under diffuse indoor daylight.[13] Various methods have been developed to synthesize carbon doped TiO_2 and enhanced visible light activity of the doped photocatalyst has been verified by many groups subsequently.[14-18] Among these methods, heating precursor containing carbon species is the most commonly used one for doping TiO_2 with carbon[19-21]. However, the existing states of carbon in these photocatalysts have triggered a lot of arguments. Carbon was proposed to substitute a lattice atom in some reports,[12, 15, 22] while interstitial carbon atoms were believed to dominate in other works.[16, 23] Recently, Kisch and co-workers have attributed the visible light activity of some "carbon-doped" TiO_2 to the sensitization of TiO_2 by aromatic carbon compound.[24] Moreover, no visible activity or detrimental effect of C doping on photocatalytic activity of TiO_2 under UV light was observed in some cases.[25-27]

Herein we report an easy way to fabricate carbon doped TiO_2 with high photocatalytic activity for hydrogen production via fast combustion of organic capping reagents. During surface modification of TiO_2 with carbon via heating oleylamine wrapped ultrathin TiO_2 nanosheets,[28] we noticed that elevating calcination temperature or heating rate in air would dope carbon into TiO_2 lattice. By varying the temperature ramp-up rates, we prepared several carbon doped TiO_2 photocatalysts. A high and stable hydrogen generation rate was observed on those prepared under a high heating rate, which benefits fast combustion of oleylamine ligands. In contrast, those prepared under a low heating rate exhibited a relative low activity under UV light and no activity under visible light. We think fast and slow combustion of oleylamine ligands may lead to different carbon doping states in the final products.

Experimental

[a] Beijing National Laboratory for Molecular Science, Key Laboratory of Photochemistry, Institute of Chemistry, Chinese Academy of Sciences, Beijing, 100190, People's Republic of China. E-mail: jnyao@iccas.ac.cn;
[b] State Key Laboratory of Material Processing and Die & Mould Technology, School of Material Sciences and Engineering, Huazhong University of Science and Technology, Wuhan, 430074, People's Republic of China. E-mail: yingma@hust.edu.cn

Materials

The following chemicals were used as received without further purification. Titanium (IV) isopropoxide ($Ti(OC_3H_8)_4$, 95%) was purchased from Alfa Aesar. Oleylamine (OAm, 70%) was purchased from Sigma Aldrich. NaOH (≥96.0%), H_2PtCl_6 (Pt ≥37.0%), Na_2SO_4 (>99%), ethanol (>99.7%), methanol (>99.5%) and hexane (>97%) were purchased from Sinopharn Chemical Reagent Co., Ltd. Deionized water was purified by using a high-purity water system (Millipore Milli-Q, resistivity>18.2 MΩ·cm) before it was used.

Synthesis of carbon-doped TiO_2 nanomaterials.

Oleylamine wrapped ultrathin TiO_2 nanosheets were first synthesized by a thermal decomposition method reported previously.[28] Carbon-doped TiO_2 nanomaterials were then prepared by calcining the as-obtained TiO_2-oleylamine nanosheet precursor in a muffle furnace (F47920-33-80, Thermo Scientific Co., USA) at different temperatures in air. For fast heating rate, TiO_2-oleylamine precursor was placed into the muffle furnace which was preheated to certain temperature, and then calcined for 0.5 (500 °C) or 1 h (400 °C). The samples produced via fast combustion are designated by F-500-0.5 and F-400-1, respectively. For normal heating process (low heating rate), the precursor was firstly heated to 300 °C at a ramp rate of 10 °C min^{-1}, held for 1 h, then heated to 450 or 500 °C and help for 1 h. The corresponding samples are denoted as N-300-450 and N-300-500, respectively.

Preparation of Pt-loaded photocatalysts

Approximately 50mg of carbon-doped TiO_2 materials was suspended with sonication in 8 mL of deionized water and 0.8 mL of H_2PtCl_6 (10 g L^{-1}) aqueous solution. The pH value of the solution was adjusted to 12 by 10 M NaOH solution. Then the suspension was stirred at 50 °C for 5 h under ambient atmosphere, followed by adding 2 mL of methanol and irradiated using a 300 W Xenon lamp for 2 h (~ 600 mW cm^{-2}, CEL-HXF300, Beijing Aulight Co., Ltd.). The Pt-loaded photocatalysts were washed with water and ethanol and centrifuged, followed by drying in an electric oven at 60 °C for overnight.

Photocatalytic hydrogen generation

An online photocatalytic hydrogen generation system (AuLight, Beijing, CEL-SPH2N) was used to conduct the photocatalytic hydrogen evolution experiments at ambient temperature (25 °C). In a typical photocatalytic experiment, 50 mg of Pt-loaded photocatalyst was suspended in 100 mL of aqueous solution containing 40% of methanol in volume. Prior to irradiation, the suspension was degassed with vacuum pump for 10 min to completely remove the dissolved oxygen and to assure the reaction system in an inertial condition. A magnetic stirrer was applied at the bottom of the reactor to keep a good dispersion of the photocatalysts throughout the whole experiment. The hydrogen evolved was analysed by gas chromatograph (GC) using a thermal conductivity detector (TCD) with nitrogen as a carrier gas. Once the photocatalytic reaction of a testing cycle in 5 h was finished, the reactor was replenished with 2 mL of methanol and degassed in vacuum before starting the subsequent cycles. The above mentioned Xenon lamp (300 W, a total light intensity of 600 mW cm^{-2}) was used as simulated light source. Visible light was acquired by equipping Xenon lamp with a 400 nm longpass filter (UVCUT400, AuLight, Beijing, λ>400 nm, ~ 550 mW cm^{-2}). The apparent quantum efficiency (QE) was measured under the same photocatalytic reaction conditions with a 365 nm (~ 90 mW cm^{-2}) and a 420 nm band-pass filter (~ 30 mW cm^{-2}). The QE was calculated according to the following equation:

$$QE[\%] = \frac{\text{number of reacted electrons}}{\text{number of incident photons}} \times 100$$

$$= \frac{\text{number of evolved } H_2 \text{ molecules} \times 2}{\text{number of incident photons}} \times 100$$

Photocurrent measurement of PEC cells

Transient photocurrent response was performed on a Zennium electrochemical workstation (ZAHNER, Germany) in a standard three-electrode system with the as-prepared samples as the working electrodes with an active area of ca. 1 cm^2, a Pt wire as the counter electrode and Ag/AgCl (saturating KCl) as the reference electrode, which includes a UV light source (365 nm) and the corresponding control system. 1 M Na_2SO_4 aqueous solution was used as the electrolyte. For working electrodes, FTO glass (2cm × 1.2 cm) was immersed in an ethanolic dispersion of carbon-doped photocatalysts and followed by drying in the air. This process was repeated several times until the coated photocatalyst reaches ca. 0.4 mg cm^{-2} on FTO glass. The amperometric *I-t* curves were recorded under an illumination of 10 mW cm^{-2} for three 50 seconds light-on-off cycles.

Characterization

The morphologies of carbon-doped photocatalysts were observed by transmission electron microscopy (TEM) images recorded using a JEOL JEM1011 TEM operated at 100 kV and high-resolution TEM (HRTEM) images recorded on a JEOL 2010F operated at 200 kV. Samples were prepared by drop-casting a dispersion drop on a 300 mesh carbon-coated copper TEM grid followed by drying at ambient atmosphere. All X-ray diffraction (XRD) patterns were recorded on a PANalytical Empyrean diffractometer equipped with a Cu Kα radiation (λ= 1.5406 Å). Each Fourier transform infrared spectrometer (FTIR) spectrum was collected on a Tensor 27 FT-IR Spectrometer (Bruker, Germany) after 32 scans at a resolution of 4 cm^{-1} from 400 to 4000 cm^{-1}. Raman spectra were obtained using a Renishaw InVia Reflex spectrometer (Wotton-under-Edge, UK), operating with an excitation laser wavelength of 532 nm. The diffraction grating gave the spectra with a spectral resolution of 2 cm^{-1}. The specific surface areas of the photocatalysts were determined by Quadrasorb SI-MP (Quantachrome Instrument). All samples were degassed at 60 °C for 10 h before N_2 adsorption. The carbon contents of the samples were investigated using an electron probe microanalyzer (EPMA) (Shimadzu, EPMA-1720, Japan). X-ray photoelectron spectroscopy (XPS) was obtained with an ESCALab220i-XL electron spectrometer using 300 W Mg Kα radiation. All binding energies were referenced to the C 1s neutral carbon

peak, which was assigned to the value of 284.8 eV to compensate for surface charge effects. Diffuse reflectance UV-visible spectra were recorded with Hitachi U-3010 spectrophotometer and photoluminescence (PL) spectra were measured at room temperature on an Edinburgh Instruments FLS920 spectrometer with 375 nm laser light source. The electron paramagnetic resonance (EPR) spectra of carbon-doped nanomaterials were recorded using

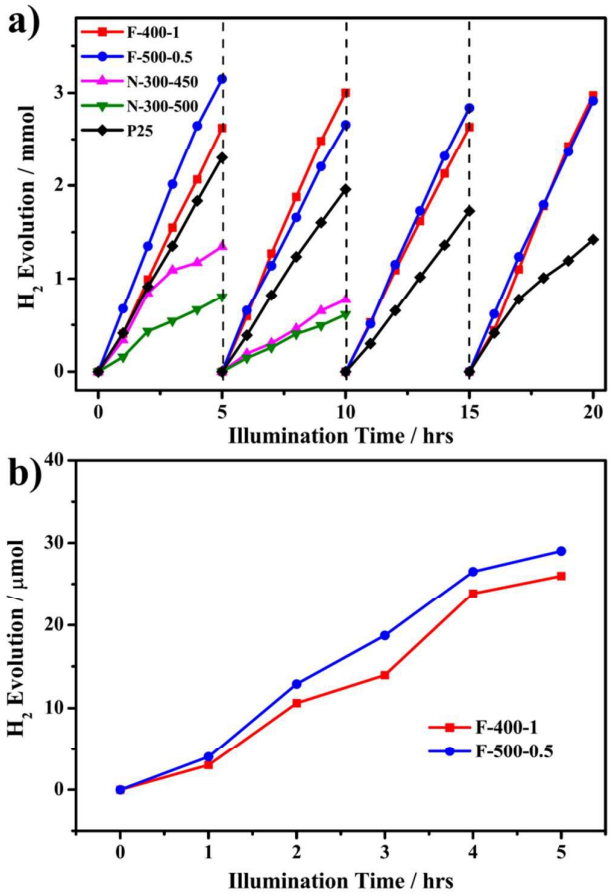

Fig. 1. Photocatalytic H_2 evolution amount against time from the photocatalysts under a) simulated solar irradiation and b) visible light irradiation (λ>400 nm). Photocatalytic experiments were performed in 40% (v/v) methanol/water solutions.

an ELEXSYS ESR spectrometer (Bruker) operating at 9.7 GHz with a modulation frequency of 50 kHz and a super-high Q microwave cavity. All ESR samples were placed in Quartz ESR tubes with an inner diameter of about 5.8 mm.

Results and discussion

All of the samples obtained after calcination of TiO_2-oleylamine nanosheet precursor in air are yellow powders in appearance, in contrast to grey powders of carbon hybrid photocatalysts we reported previously,[28] no matter high or low heating rate was used. However, the activity of these photocatalysts differs from one another significantly. Photocatalytic H_2-production activity was evaluated under simulated solar irradiation using methanol as a sacrificial reagent and Pt as co-catalyst. All the measurements were carried out in an online photocatalytic hydrogen generation system at ambient temperature. Hydrogen production rates from the suspensions with different photocatalysts as a function of time are shown in Fig. 1a. The rates of hydrogen production calculated for F-400-1 and F-500-0.5 are 621 μmol·h^{-1} and 676μmol·h^{-1}, respectively. The stability of these two photocatalysts was also tested by repeating photocatalytic experiments. After four cycles, both the photocatalysts exhibit no significant loss in activity, indicating their good stability in photocatalytic hydrogen production. In contrast, the hydrogen production rate over N-300-450 is around 338 μmol·h^{-1} in the first 1 h, but decreases quickly to 212 μmol·h^{-1} in the second cycle. Similar behaviour and slower hydrogen evolution than that of N-300-450 can be observed for N-300-500. It is apparently that F-400-1 and F-500-0.5 show much higher and more stable photocatalytic activity for water splitting than N-300-450 and N-300-500. Photocatalytic experiment of commercial P25 powders was also tested and the results are shown in Fig. 1a for comparison. In otherwise identical condition, P25 powders present a slightly lower hydrogen evolution rate than those of fast heating process derived photocatalysts. More importantly, evolved hydrogen from water in P25 suspension decreases gradually with increasing the illumination time. The photocatalytic hydrogen production rates under visible light (λ>400 nm) over these carbon doped TiO_2 samples were also measured by equipping the light source with a 400 nm longpass filter, and the results are shown in Fig. 1b. Only the fast heating process derived photocatalysts exhibit visible light activity. Hydrogen evolution rates from samples F-400-1 and F-500-0.5 are detected as 5.2 and 5.9 μmol·h^{-1}, respectively. No hydrogen was detected from water with N-300-450 and N-300-500 after 5 h illumination. The apparent quantum efficiencies of F-500-0.5 are calculated to be 6.02% at 365 nm and 0.14% at 420 nm.

To better understand the key factors leading to such a difference in activity among these carbon doped TiO_2 photocatalysts, detailed structural analyses were carried out. The crystalline structures of the photocatalysts were confirmed by powder XRD patterns (shown in Fig. 2a). The peaks at 25.52°, 48.01°, 53.96°, 55.04° and 62.68° can be assigned to the (101), (004), (200), (105), (211) and (204) planes of anatase (space group: $I4_1/amd$; tetragonal symmetry, a = 3.7852Å, c = 9.5139 Å, JCPDS card no. 21-1272), respectively.[29] No diffraction peaks belonging to potential impurities, rutile or brookite can be discerned. According to the half-width at half maximum (FWHM) of (101) peaks of F-400-1, F-500-0.5, N-300-450 and N-300-500, the crystallite size of anatase estimated using the Scherrer equation are about 11.0, 12.4, 13.2, 14.2 nm, respectively. The crystallite size slightly increases with the rise of calcination temperature and the prolongation of calcination time.

Fig. 2b shows the FTIR spectra of the photocatalysts. The characteristic absorption bands of adsorbed water molecules including stretching vibration ranging from 3200 to 3400 cm^{-1} and bending vibration at around 1633 cm^{-1} are clearly visible in

all samples, indicating that water is adsorbed on their surface.[30] The strong absorption band at *ca.* 462 cm^{-1} originates from the vibration of Ti-O bonds, and the absorption bands at 1384 cm^{-1} can be assigned to O-H in-plane

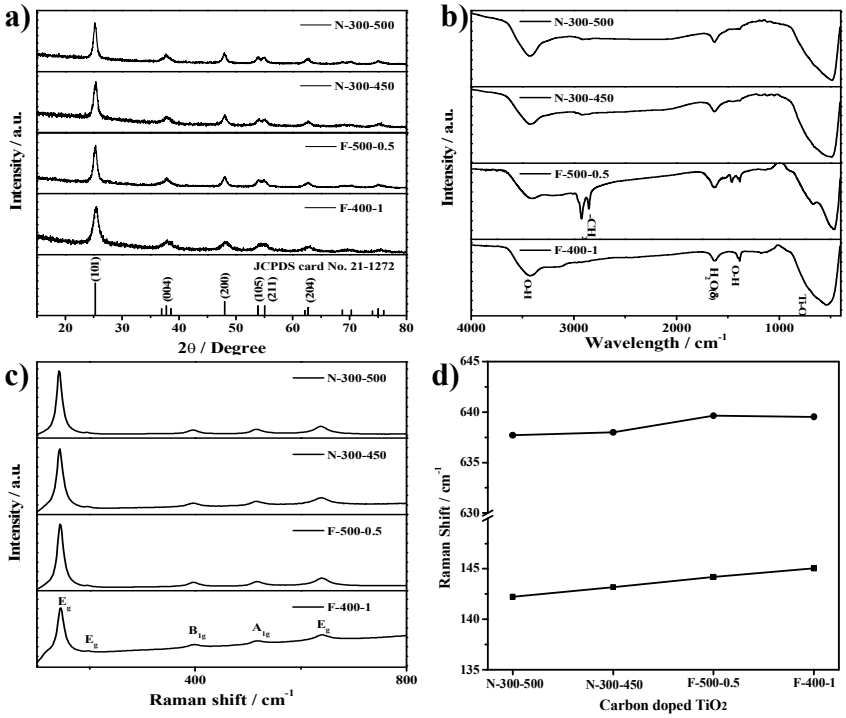

Fig. 2. (a) XRD patterns, (b) IR spectra, (c) Raman spectra and (d) Raman shifts of Eg modes of the photocatalysts.

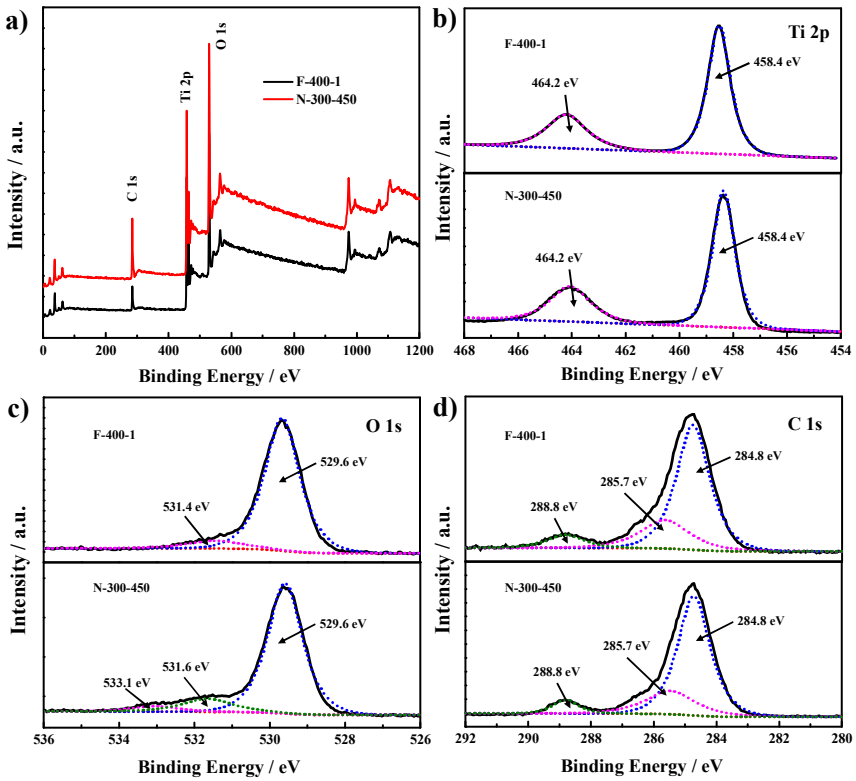

Fig. 3. XPS spectra of F-400-1 and N-300-450: (a) survey, (b) Ti 2p, (c) O1s and (d) C 1s spectra.

deformation. The latter becomes weaker when high calcination temperature or long calcination time was adopted. The emergence of absorption bands at 2923, 2853 and 1463 cm^{-1}, assigned to ν_{as} (-CH_2), ν_s (-CH_2) and δ_{as} (-CH_2), suggests the existence of trace organic residue in sample F-500-0.5 due to short time combustion.[31] Raman spectroscopy is a powerful non-destructive technique for the investigation of the crystalline quality of photocatalysts. Six typical Raman-activevibrational modes of anatase have been reported including modes A_{1g} (513 cm^{-1}), B_{1g} (399 and 519 cm^{-1}), and E_g (144, 197 and 639 cm^{-1}).[32] All the Raman peaks shown in Fig. 2c correspond to these vibrational modes, indicating that anatase is the predominant phase structure in the photocatalysts. The blue shift in E_g modes of F-500-0.5 and F-400-1 (Fig. 2d) may be attributed to more defects generated in fast combustion and crystallization process.

To investigate the chemical states of carbon atoms incorporated into the TiO_2 photocatalysts, X-ray photoelectron spectroscopy (XPS) was also utilized to record the Ti 2p, O 1s and C 1s elements of the photocatalysts. Similar XPS spectra were obtained for all the photocatalysts including P25 and typical spectra are shown in Fig. 3 for clarity. As shown in Fig. 3a, the survey spectra of all photocatalysts exhibit all peaks of elements of Ti, O and C. In Fig. 3b, two intense symmetric peaks at 458.4 and 464.2 eV in Ti 2p spectra of F-400-1 and N-300-450 can be ascribed to Ti $2p_{3/2}$ and Ti $2p_{1/2}$, respectively. The ΔE value between Ti $2p_{3/2}$ and Ti $2p_{1/2}$ was about 5.8 eV, indicating that the element of Ti in photocatalysts is predominantly Ti^{4+}.[33] The main peak at 529.6 eV in O 1s spectra of photocatalysts (Fig. 3c) can be assigned to O in the form of the O-Ti bond (lattice O), while the peak at 531.4 eV can be assigned to C=O bond (and COO).[34] The peak at around 533.1 eV of N-300-450 and P25 (not shown here) may be caused by hydroxyl groups and chemisorbed water.[35, 36] For the C 1s spectra shown in Fig. 3d, peaks at 284.8, 285.7 and 288.8 eV can be attributed to the C-C neutral bond, C-OR(H) group and COO or COOR(H) group, respectively,[34] since nearly the same C1s spectrum was obtained for all samples including P25. These oxidised carbon species originate from the incomplete combustion of organic molecules in the TiO_2-oleylamine precursor or adventitious hydrocarbonaceous and carbonate species[18]. No peak at 281.8 eV can be discerned, as usually observed for carbon-doped TiO_2 prepared by heating a carbon-containing precursor[19-21]. This cannot exclude oxygen substitution of carbon to form a Ti-C bond because this peak often appears after surface cleaning by Ar^+ sputtering.[18, 37] Although the carbon doped photocatalysts exhibit different O1s XPS spectra, the different surface oxygen species seem to have little effect on their photocatalytic activities for hydrogen evolution. Both N-300-450 and N-300-500 show low activity, but surface oxygen species related to 533.1 eV was only observed in N-300-450. In addition, weak signals of N1s were detected (Fig. S1) and the nitrogen contents were estimated by XPS analyses to be 0.66, 0.79, 0.54 and 0.49 atom% for F-400-1, F-500-0.5, N-300-450 and N-300-500, respectively. The carbon doping contents of F-400-1, F-500-0.5, N-300-450 and N-300-500 are about 1.65, 1.78, 1.60 and 1.48 atom%, respectively, determined by EPMA. No nitrogen contents were detected by EPMA, indicating trace nitrogen exits only on the surface of these samples.

According to the above XPS spectra and other structural analyses, no obvious structural difference seems to contribute to different photocatalytic behaviour observed on the samples prepared by slow and fast combustion processes. The morphologies of carbon-doped photocatalysts were further confirmed by TEM and HRTEM techniques. TEM images of these photocatalysts (Fig. 4) show that the samples are composed of nanoparticles with sizes of 5~15 nm. As clearly observed in HRTEM images, the (101) planes of these carbon-doped anatase particles are well-defined, indicating the well crystallinity of the photocatalysts. The average size of the photocatalysts increases slightly with the temperature

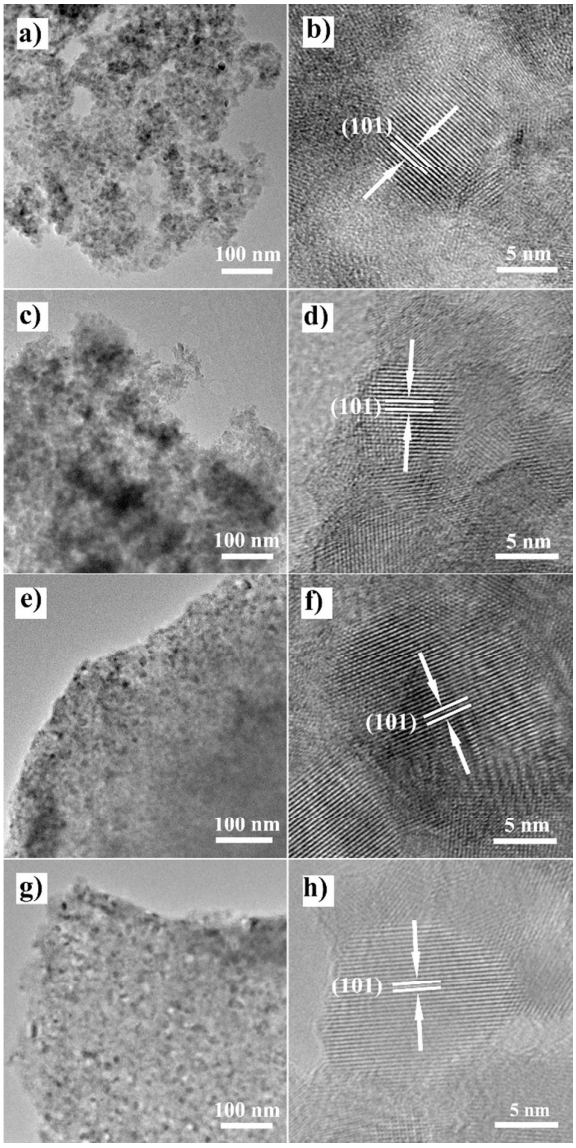

Fig. 4. TEM and HRTEM images of F-400-1 (a and b), F-500-0.5 (c and d), N-300-450 (e and f) and N-300-500 (g and h).

elevating and the calcination time prolonging, which is consistent with the result obtained from the XRD patterns. In particular, the polydispersity of the nanoparticles increases significantly during slow heating process. Furthermore, these nanoparticles seem to aggregate more severely, as shown in Fig. 4e and 4g. Better dispersion and less aggregation of nanoparticles in both F-samples may benefit their high photocatalytic activity, whereas the BET surface areas determined by N_2 adsorption experiments are *ca.* 96, 69, 72 and 59 $m^2\ g^{-1}$ for F-400-1, F-500-0.5, N-300-450 and N-300-500, respectively. In fact, F-500-0.5 and N-300-450 exhibit very different activities although they possess similar surface areas, while both F-samples show similar activities instead.

UV-Vis diffuse reflectance absorption spectroscopy was utilized to characterize the optical property of the photocatalysts, and the absorption spectrum of commercial P25 was also shown for comparison. As illustrated in Fig. 5a, All the samples exhibit typical intense absorption in the UV region, mediated by the intrinsic bandgap absorption of TiO_2 resulting from the electron transitions from the valence band to the conduction band ($O_{2p} \rightarrow Ti_{3d}$). Compared to P25, redshift of absorption onset is obviously observed in all of the carbon-doped photocatalysts with only anatase phase, which corresponds to the narrow of bandgap energy. As a well-known indirect semiconductor, the bandgap energy (E_g) of TiO_2 can be calculated from the intersection of the extrapolated linear portion in the plot of $(\alpha h\nu)^{1/2}$ versus the photon energy

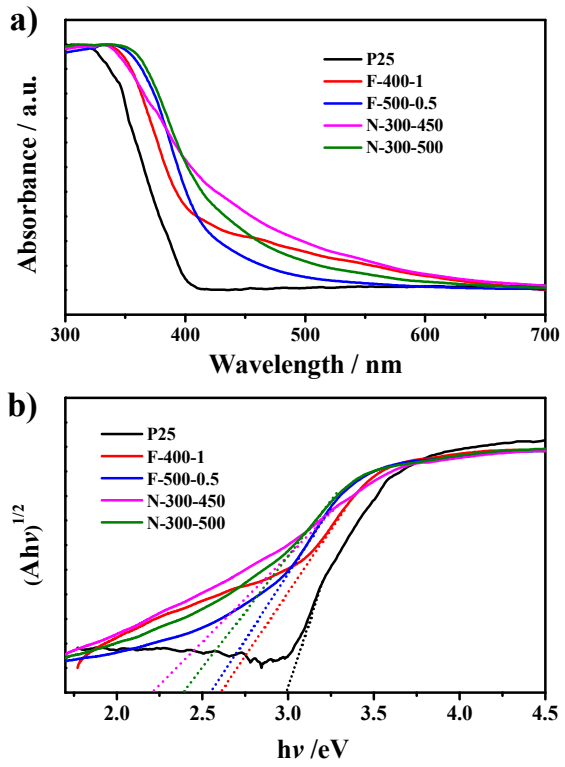

Fig. 5. (a) UV-vis diffuse reflectance spectra of the carbon doped TiO_2 and commercial P25; (b) plot of $(Ah\nu)^{1/2}$ versus photon energy (eV).

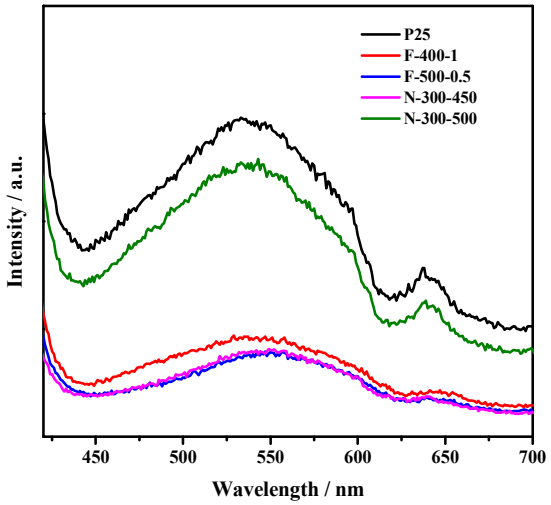

Fig. 6. Photoluminescence emission spectra of the photocatalysts.

($h\nu$) following the equation[16]: $(\alpha h\nu)^{1/2} \propto h\nu - E_g$, where ($\alpha$) is the optical absorption coefficient and linearly proportional to the absorbance (A). As shown in Fig. 5b, the bandgap of all carbon-doped photocatalysts is narrower (F-400-1, 2.62 eV; F-500-0.5, 2.55 eV; N-300-450, 2.0 eV; N-300-500, 2.4 eV; respectively) than that of P25 (3.0 eV). It has been well accepted that doping TiO_2 with carbon can effectively decrease the bandgap of TiO_2 although the electronic structure of carbon doped TiO_2 is still a matter of disputation[24, 38, 39]. In addition, the visible absorbance of TiO_2 is significantly strengthened after carbon doping as evidenced by a long tail absorption in the visible range in Fig. 5a.

PL emission spectra have been widely used to investigate the efficiency of charge carrier trapping, migration, and transfer and to understand the recombination of free charge carriers in semiconductor particles. In this study, the PL emission spectra of all samples were examined with an Edinburgh Instruments FLS920 spectrometer equipped with a 375 nm continuous laser as the excitation light source. As shown in Fig. 6, an intense peak at about 530 nm (2.34 eV) with a broad spectral width can be observed for all samples, which has been detected in many TiO_2 photocatalysts and attributed to the charge transfer from Ti^{3+} to the oxygen anion in a TiO_6^{8-} complex.,[40, 41] while the weak luminescence at about 640 nm (1.94 eV) might be a consequence of the Frank-Condon principle and the polarizability of the lattice ions surrounding the vacancy[42] or originate from the radiative recombination of excitons trapped to surface and subsurface defects.[43] Close inspection of these spectra reveals a small shift of the emission peaks toward the longer wavelength region and a decrease in emission intensity in the carbon doped TiO_2 samples except for N-300-500. The decrease in emission intensity suggests that the doping of carbon into TiO_2 leads to the efficient quenching of the photoluminescence with different efficiencies. Similar quenching in the luminescence intensity has also been observed for In,[44] F,[40] and N[8] doped TiO_2. Consequently, separation efficiency of the

photoinduced electron and hole and thus the photocatalytic activity of the photocatalysts for water splitting may be enhanced. It should be noted that N-300-450 exhibits low activity although weak PL was also observed, which may be due to nonradiative recombination of charge carriers. This indicates different carbon states possibly exist in N-300-450 from those in F-400-1 and F-500-0.5.

It is reported that photocurrent response mainly depends on the photoelectron generation, electron-hole pair separation and the electron-transfer efficiency on the surface of a semiconductor catalyst. In a sense, responsive photocurrent intensity could reflect the overall photoelectron conversion efficiency. To further understand the enhanced photocatalytic activity of both F-samples, the transient photocurrent on-off cycles of intermittent UV-light irradiation (365nm) with 10 mW cm^{-2} light density. As can be obviously seen from the figure, an

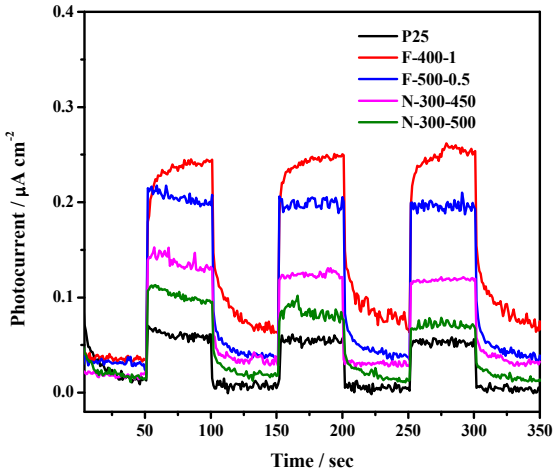

Fig. 7. Transient photocurrent responses of the photocatalysts for three 50 s light-on-off cycles in 1 M Na_2SO_4 aqueous solution under UV light irradiation with a bias potential of 0.5V.

apparent rise in the photocurrent responses can be discerned for all the electrodes, when the light is on, and the on-off cycles of the photocurrents are reproducible. We assume that the photocurrent should be attributed to the generation and separation of photo-generated electron-hole pairs at the TiO_2/electrolyte interface. Holes move to the surface of TiO_2, where they are trapped or captured by reduced species in the electrolyte, while the electrons are transported to the back contact substrate *via* TiO_2. Under dark conditions, the weak dark currents at an anodic potential of 0.5 V may result from pure electrochemical reaction on carbon-doped TiO_2 electrodes.

Further observation indicates that the photocurrents of F-400-1 and F-500-0.5 are higher than those of N-300-450 and N-300-500. A higher photocurrent response means a lower electron–hole recombination and a higher photoelectron transfer efficiency, which may contribute to higher photocatalytic activity of the photocatalysts. Except for P25, the order of photocurrent intensities is nearly consistent with that of photocatalytic activity for carbon doped TiO_2 (Fig. 1). Although N-300-450 exhibits very weak photoluminescence (Fig. 6), its photocurrent at 0.5V is much lower than that of F-samples, suggesting its low efficiency in electron-hole pair separation. Lowest photocurrent was observed on P25 electrode, manifesting poorer photogenerated charge separation in P25 than that in carbon doped samples. In other words, carbon doping seems to be favourable for charge separation.

Striking difference of these photocatalysts can be easily detected by electron spin resonance (ESR) investigations at room temperature. ESR/EPR is used to characterize the unpaired electrons or paramagnetic centers such as Ti^{3+} and oxygen vacancy (one electron trapped) in TiO_2 crystals.[19, 45, 46] As shown in Fig. 8, F-400-1 gave rise to a very strong EPR signal at about g = 2.005, which has been attributed to a single-electron trapped oxygen vacancy.[27] A weak signal was also observed for F-500-0.5, while an even weaker signal or no

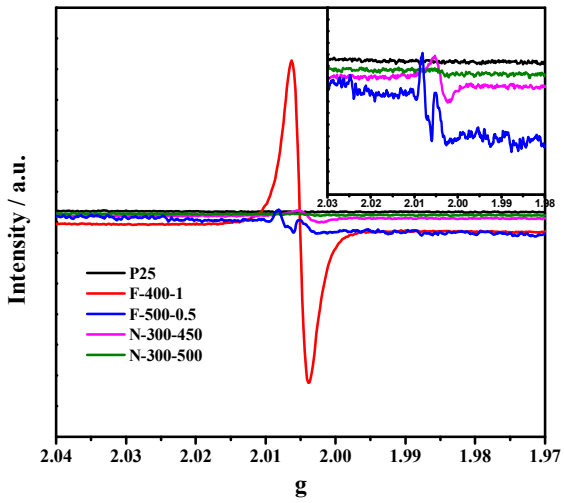

Fig. 8. EPR spectra of TiO_2 photocatalysts at room temperature operating at 9.7 GHz. Inset shows the enlarged weak signals.

signal was seen for N-samples and P25. The absence of EPR signal at g < 2.0 indicates the absence of the Ti^{3+} spins. EPR results demonstrate that fast heating process may favour the generation of oxygen vacancies as TiO_2 is doped by carbon. For the same heating rate, the lower calcination temperature used, the more oxygen vacancies generated, similar to EPR signals of Co doped TiO_2 B nanotubes reported previously.[47]

As complexity of carbon doping states in TiO_2 is concerned, many theoretical discussions have been reported based on density functional theory (DFT) calculations.[38, 39, 48] Our experimental results have been supported by previous theoretical calculations. Valentin et al.[49] predicted that carbon may be substituted for oxygen and oxygen vacancies would be formed under oxygen-poor conditions, while carbon may be substituted for Ti or situated in an interstice under oxygen-rich conditions when carbon concentration is relatively low. In this work, the atmosphere should be deficient in oxygen during fast combustion of oleylamine, while slow combustion of oleylamine may give rise to an atmosphere with richer oxygen.

As a result, substitutional carbon atoms and oxygen vacancies are favoured when carbon is doped at a high heating rate, whereas, few oxygen vacancies will be formed at a normal heating rate. More importantly, such different doping states seem to have a great effect on photocatalytic activity toward water splitting of the carbon doped TiO_2 nanomaterials. In comparison to pure TiO_2 nanoparticles prepared by the same precursor reported in our previous work (hydrogen production rate of ~ 50 $\mu mol \cdot h^{-1}$ in first 10 h),[28] the photocatalytic activity for all of the carbon doped TiO_2 nanomaterials here is enhanced more or less. As compared with P25, a commercial TiO_2 photocatalyst with mixed phases of anatase and rutile, improved photogenerated electron-hole pair separation in N-samples has been demonstrated via PL and photocurrent responses, whereas, N-samples presented lower activity than P25, which may be due to aggregation of nanoparticles during calcination (Fig. 4) and loss of surface active sites. In particular, the significant improvement in photocatalytic activity can be only realized when oxygen vacancies are formed in TiO_2 during carbon doping. Such carbon doped TiO_2 photocatalysts (F-samples herein) exhibited superior photocatalytic performance to P25. Moreover, high photocatalytic activity of F-samples remains after 20 h irradiation, in contrast to gradual decrease in activity for P25 and N-samples. According to previous investigations, intermediates produced during photocatalytic reaction will block active sites of the photocatalyst and result in its deactivation. When methanol is used as a sacrificial reagent in this work, enhanced electron-hole separation and more O-H species on surface evinced by FTIR spectra (Figure 2b) in fast combustion samples may benefit complete oxidation of methanol to CO_2. This possibly avoids the blockage of the active sites and high stability of these fast combustion samples are observed as a result.

Conclusions

In summary, we have demonstrated fast combustion of organic carbon species in precursor is a simple and effective method for fabrication of carbon doped TiO_2 photocatalysts with high and stable photocatalytic activity for hydrogen production. Fast calcination process not only offers an oxygen-poor atmosphere to benefit carbon doping and oxygen vacancies forming, but also avoids aggregation of the nanoparticles in some sense. Excellent photocatalytic property can be thus obtained in the final product. In contrast, slow calcination process derived carbon doped TiO_2 show lower activity, which further decreases with prolonging illumination time. This variation in temperature ramp-up rates during calcination may be extended to control doping states of other elements to better modify the properties of semiconductors.

Acknowledgements

This work was supported by the National Natural Science Foundation of China (no. 21273249), National Basic Research Program of China (no. 2011CB808402), and Huazhong University of Science and Technology.

Notes and references

1. A. L. Linsebigler, G. Lu and J. T. Yates, *Chem. Rev.*, 1995, **95**, 735-758.
2. H. Chen, C. E. Nanayakkara and V. H. Grassian, *Chem. Rev.*, 2012, **112**, 5919-5948.
3. R. Asahi, T. Morikawa, H. Irie and T. Ohwaki, *Chem. Rev.*, 2014, **114**, 9824-9852.
4. S. Rawalekar and T. Mokari, *Adv. Energy Mater.*, 2013, **3**, 12-27.
5. W. Hou and S. B. Cronin, *Adv. Funct. Mater.*, 2013, **23**, 1612-1619.
6. Y. Ma, X. Wang, Y. Jia, X. Chen, H. Han and C. Li, *Chem. Rev.*, 2014, **114**, 9987-10043.
7. T. Hisatomi, J. Kubota and K. Domen, *Chem. Soc. Rev.*, 2014, **43**, 7520-7535.
8. R. Asahi, T. Morikawa, T. Ohwaki, K. Aoki and Y. Taga, *Science*, 2001, **293**, 269-271.
9. Y. Li, Y. Jiang, S. Peng and F. Jiang, *J. Hazard. Mater.*, 2010, **182**, 90-96.
10. Y. Li, G. Ma, S. Peng, G. Lu and S. Li, *Appl. Surf. Sci.*, 2008, **254**, 6831-6836.
11. Y. Li, C. Xie, S. Peng, G. Lu and S. Li, *J. Mol. Catal. A: Chem.*, 2008, **282**, 117-123.
12. S. U. M. Khan, M. Al-Shahry and W. B. Ingler, *Science*, 2002, **297**, 2243-2245.
13. S. Sakthivel and H. Kisch, *Angew. Chem. Int. Ed.*, 2003, **42**, 4908-4911.
14. H. Irie, Y. Watanabe and K. Hashimoto, *Chem. Lett.*, 2003, **32**, 772-773.
15. J. H. Park, S. Kim and A. J. Bard, *Nano Lett.*, 2006, **6**, 24-28.
16. G. Wu, T. Nishikawa, B. Ohtani and A. Chen, *Chem. Mater.*, 2007, **19**, 4530-4537.
17. D.-e. Gu, Y. Lu, B.-c. Yang and Y.-d. Hu, *Chem. Commun.*, 2008, **8**, 2453-2455.
18. S.-i. In, A. H. Kean, A. Orlov, M. S. Tikhov and R. M. Lambert, *Energy Environ. Sci.*, 2009, **2**, 1277-1279.
19. Y. Li, D.-S. Hwang, N. H. Lee and S.-J. Kim, *Chem. Phys. Lett.*, 2005, **404**, 25-29.
20. H. J. Yun, H. Lee, J. B. Joo, N. D. Kim, M. Y. Kang and J. Yi, *Appl. Catal. B: Environ.*, 2010, **94**, 241-247.
21. B. Liu, L.-M. Liu, X.-F. Lang, H.-Y. Wang, X. W. Lou and E. S. Aydil, *Energy Environ. Sci.*, 2014, **7**, 2592-2597.
22. H. Wang, Z. Wu and Y. Liu, *J. Phys. Chem. C*, 2009, **113**, 13317-13324.
23. E. Barborini, A. M. Conti, I. Kholmanov, P. Piseri, A. Podestà, P. Milani, C. Cepek, O. Sakho, R. Macovez and M. Sancrotti, *Adv. Mater.*, 2005, **17**, 1842-1846.
24. P. Zabek, J. Eberl and H. Kisch, *Photochem. Photobiol. Sci.*, 2009, **8**, 264-269.
25. T. Tachikawa, S. Tojo, K. Kawai, M. Endo, M. Fujitsuka, T. Ohno, K. Nishijima, Z. Miyamoto and T. Majima, *J. Phys. Chem. B*, 2004, **108**, 19299-19306.
26. T. Sano, E. Puzenat, C. Guillard, C. Geantet and S. Matsuzawa, *J. Mol. Catal. A: Chem.*, 2008, **284**, 127-133.
27. I.-C. Kang, Q. Zhang, S. Yin, T. Sato and F. Saito, *Appl. Catal. B: Environ.*, 2008, **80**, 81-87.
28. Y. Yang, Y. Yao, L. He, Y. Zhong, Y. Ma and J. Yao, *J. Mater. Chem. A*, 2015, **3**, 10060-10068.
29. X. Shao, W. Lu, R. Zhang and F. Pan, *Sci. Rep.*, 2013, **3**.

30. Y. Sun, X. Hu, W. Luo and Y. Huang, *J. Mater. Chem.*, 2012, **22**, 19190-19195.
31. C. Hontoria-Lucas, A. J. López-Peinado, J. d. D. López-González, M. L. Rojas-Cervantes and R. M. Martín-Aranda, *Carbon*, 1995, **33**, 1585-1592.
32. L.-W. Zhang, H.-B. Fu and Y.-F. Zhu, *Adv. Funct. Mater.*, 2008, **18**, 2180-2189.
33. Z. Song, J. Hrbek and R. Osgood, *Nano Lett.*, 2005, **5**, 1327-1332.
34. J. Liu, Q. Zhang, J. Yang, H. Ma, M. O. Tade, S. Wang and J. Liu, *Chem. Commun.*, 2014, **50**, 13971-13974.
35. C. D. Wagner, D. A. Zatko and R. H. Raymond, *Anal. Chem.*, 1980, **52**, 1445-1451.
36. C. Ammon, A. Bayer, H. P. Steinrück and G. Held, *Chem. Phys. Lett.*, 2003, **377**, 163-169.
37. W. Zhongbiao, D. Fan, Z. Weirong, W. Haiqiang, L. Yue and G. Baohong, *Nanotechnology*, 2009, **20**, 235701.
38. J. Lu, Y. Dai, M. Guo, L. Yu, K. Lai and B. Huang, *Appl. Phys. Lett.*, 2012, **100**, 102114.
39. K. Yang, Y. Dai, B. Huang and M.-H. Whangbo, *J. Phys. Chem. C*, 2009, **113**, 2624-2629.
40. J. C. Yu, J. Yu, W. Ho, Z. Jiang and L. Zhang, *Chem. Mater.*, 2002, **14**, 3808-3816.
41. B. Gao, Y. Ma, Y. Cao, W. Yang and J. Yao, *J. Phys. Chem. B*, 2006, **110**, 14391-14397.
42. D. Li, H. Haneda, S. Hishita and N. Ohashi, *Chem. Mater.*, 2005, **17**, 2596-2602.
43. J. Zhang, X. Chen, Y. Shen, Y. Li, Z. Hu and J. Chu, *Phys. Chem. Chem. Phys.*, 2011, **13**, 13096-13105.
44. H. Tang, H. Berger, P. E. Schmid, F. Lévy and G. Burri, *Solid State Commun.*, 1993, **87**, 847-850.
45. N. Liu, C. Schneider, D. Freitag, M. Hartmann, U. Venkatesan, J. Müller, E. Spiecker and P. Schmuki, *Nano Lett.*, 2014, **14**, 3309-3313.
46. T. Su, Y. Yang, Y. Na, R. Fan, L. Li, L. Wei, B. Yang and W. Cao, *ACS Appl. Mater. Interfaces*, 2015, **7**, 3754-3763.
47. X. Wang, X. Gao, G. Li, L. Gao, T. Yan and H. Y. Zhu, *Appl. Phys. Lett.*, 2007, **91**, 143102-143102.
48. W. Hao and P. L. James, *J. Phys.: Condens. Matter.*, 2005, **17**, L209.
49. C. Di Valentin, G. Pacchioni and A. Selloni, *Chem. Mater.*, 2005, **17**, 6656-6665.

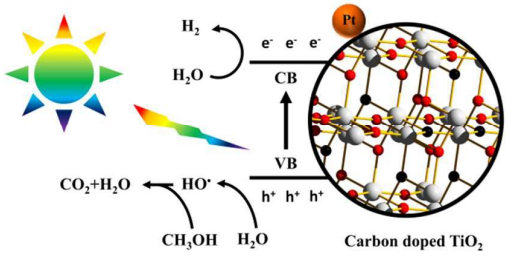

Carbon doped TiO_2 prepared by fast combustion of oleylamine ligands exhibit much higher photocatalytic activity for hydrogen production than those prepared by conventional methods.